(2)

ARMY RESEARCH LABORATORY

Deformation Mechanisms in Tungsten Single Crystals in Ballistic Impact Experiments

W. J. Bruchey, Jr.
R. N. Herring
P. W. Kingman
E. J. Horwath

ARL-TR-133 May 1993

NOTICES

REPORT DOCUMENTATION PAGE

Form Approved
OMB No. 0704-0188

1. AGENCY USE ONLY *(Leave blank)*	2. REPORT DATE	3. REPORT TYPE AND DATES COVERED
	May 1993	Final, 1 Oct 91 - 30 Sep 92

4. TITLE AND SUBTITLE

Deformation Mechanisms in Tungsten Single Crystals in Ballistic Impact Experiments

5. FUNDING NUMBERS

PR: 1L162618AH80

6. AUTHOR(S)

W. J. Bruchey, Jr., R. N. Herring, P. W. Kingman, and E. J. Horwath

7. PERFORMING ORGANIZATION NAME(S) AND ADDRESS(ES)

U.S. Army Research Laboratory
ATTN: AMSRL-WT-TA
Aberdeen Proving Ground, MD 21005-5066

8. PERFORMING ORGANIZATION REPORT NUMBER

9. SPONSORING/MONITORING AGENCY NAME(S) AND ADDRESS(ES)

U.S. Army Research Laboratory
ATTN: AMSRL-OP-CI-B (Tech Lib)
Aberdeen Proving Ground, MD 21005-5066

10. SPONSORING/MONITORING AGENCY REPORT NUMBER

ARL-TR-133

11. SUPPLEMENTARY NOTES

12a. DISTRIBUTION/AVAILABILITY STATEMENT

Approved for public release; distribution is unlimited.

12b. DISTRIBUTION CODE

13. ABSTRACT *(Maximum 200 words)*

The performance of tungsten single crystals in ballistic impact varies stongly as a function of crystallographic orientation. The deformation structure of recovered single crystal rods fired in ballistic environments has been characterized by optical microscopy, SEM and TEM, and x-ray diffraction. The observed microstructures are varied and provide substantial insights into the factors governing the penetration and flow behavior under ballistic conditions. Crystallographic orientation influences the potential for developing shear which enhances material flow, and this enhancement ultimately maximizes the energy available for target penetration. Microstructural analysis elucidates the various mechanisms occuring during the flow process for single crystals of high-symmetry orientations, and suggests possible analogies between the penetration behavior of the tungsten single crystals and other materials.

14. SUBJECT TERMS

crystallography; strain rate; dislocations; mass transfer; shear stresses

15. NUMBER OF PAGES

27

16. PRICE CODE

17. SECURITY CLASSIFICATION OF REPORT	18. SECURITY CLASSIFICATION OF THIS PAGE	19. SECURITY CLASSIFICATION OF ABSTRACT	20. LIMITATION OF ABSTRACT
UNCLASSIFIED	UNCLASSIFIED	UNCLASSIFIED	UL

INTENTIONALLY LEFT BLANK.

TABLE OF CONTENTS

INTENTIONALLY LEFT BLANK.

LIST OF FIGURES

INTENTIONALLY LEFT BLANK.

ACKNOWLEDGMENT

The authors would like to acknowledge the assistance of Mr. David MacKenzie, Terminal Effects Division, U.S. Army Research Laboratory, in sample preparation, microphotography, and timely preparation of target blocks for sectioning.

INTENTIONALLY LEFT BLANK.

1. INTRODUCTION

The material processes involved during the penetration of a long rod into a target block are not well understood. In a previous paper (Bruchey, Horwath, and Kingman 1991) presented at the 120th TMS Annual Meeting in February 1991, the ballistic results obtained from experiments using tungsten single crystal penetrators of high symmetry orientations fired into finite and semi-infinite steel target blocks were presented along with some preliminary metallographic observations of the residual penetrators. More detailed analysis is now available and will be discussed in this report.

Large-caliber penetrators used in modern day tank gun ammunition rely on the penetration performance of high-density alloys. These efforts have historically centered on the uranium and tungsten containing alloys. The uranium research has dealt with evaluations of most of the binary alloys such as U-0.75Ti and U-2Mo. Tungsten research has centered on the W-Ni-Fe alloys/composites. Both categories of materials have densities greater than 17.

In recent years, there has been considerable interest in developing tungsten materials which could be used as a substitute for uranium materials. As a precursor to tungsten alloy development, a better understanding of how the constituents of these alloys/composites behave under ballistic impact condition is required. To address this issue, a small (geometrical) scale program was initiated to assess the flow and failure behavior of single crystal tungsten rods against various target geometries. As previously reported, the single crystals of tungsten in three orientations, [111], [110], and [100], were obtained commercially and were grown using the Czochralski (CZ) technique after preliminary two pass zone refinement of 99.99% purity starting material.

The ballistic experiments have been described in detail previously. Only the principal results pertinent to the following discussion will be summarized here. Model long rod penetrators of 6.90 mm diameter and 102.5 mm length were prepared from tungsten single crystals of high symmetry orientations ([100], [111], and [110]) and fired into steel target blocks at a velocity of 1,500 m/s. In each case, the crystal axis was aligned parallel to the rod axis. A summary of the average penetration results for each of the penetrators fired into semi-infinite steel blocks is listed in Table 1. The penetration performance was found to vary

Table 1. Penetration Test Summary for Rods Fired Into Semi-Infinite Blocks of RHA Steel

MATERIAL	PENETRATION/UNIT ROD LENGTH P/L
93W-Ni-Fe Ordnance Alloy	0.84
U-0.75Ti Ordnance Alloy	0.95
[111] W Single Crystal	0.88
[110] W Single Crystal	0.83
[100] W Single Crystal	0.97

with orientation, with [100] providing the best penetration and [110] the poorest. Of particular interest, the [100] orientation outperformed a comparison 93-WHA rod in the same test and matched the performance of the U-0.75Ti grade ordnance alloy. An extended description of the ballistic tests and data analysis is contained in the previous reference. Initial macroscopic examination of polished sections of the rod embedded in the semi-infinite target blocks showed that all of the single crystal penetrators had deformed by eversion. The material at the front of the penetrator back-extruded to form a continuous hollow tube extending back along the cavity from the small residual slug at the end of the cavity. The exterior surface of the hollow tube was essentially continuous, but the interior (concave) surface was covered with a regular pattern of exfoliation. The detailed flow pattern for each orientation was quite different and the effect of orientation was observed not only in the region immediately surrounding the nose of the residual penetrator, but in the foliation pattern within the extruded tube as well. Apparent differences in the amount of shear localization as a function of orientation were concluded to be a major factor in the partition of energy during penetration and flow. However, it was apparent that further investigation of the microstructure was necessary to further elucidate the material processes.

2. MICROSTRUCTURAL INVESTIGATION - OPTICAL MICROSCOPY AND X-RAY DIFFRACTION

The previously sectioned crystals embedded in the semi-infinite target blocks were subsequently etched and examined metallographically. The sections were also x-rayed using

a standard back-reflection technique in order to determine the crystal orientation and a general indication of lattice distortion, polygonization, and recrystallization. Portions of the samples were then sectioned and thinned for transmission electron microscopy to determine the dislocation structure. In addition, a limited amount of scanning electron microscopy was performed on segments of the back-extruded material which separated from the main specimen.

The [110] penetrator, which achieved the poorest penetration, flowed in a very inhomogeneous and asymmetric manner with extensive lattice rotation. Figure 1 shows the wavy, bifurcated deformation bands typically observed in the flowed region. The remnant residual rod cracked and fractured into large fragments rotated with respect to one another. X-ray patterns in the flowed portion indicate extensive recrystallization. In some regions, strong deformation textures occur, while in others, sharp reflections from freshly recrystallized grains are observed.

Figure 1. Optical Micrograph of Wavy Bifurcated Shear Bands in [110] Penetrator.

The flowed material from the [111] penetrator also contained deformation bands, often with small regions of parent single crystal material entrained between the bands (Figure 2). Unlike the [110], a distinct rod remnant approximately equal in length to the rod diameter remained. The only visible deformation features within this residual rod are several narrow bands running from the edge of the rod into the interior (Figure 3). Separation of material from the end of the rod was probably initiated by the formation of these shear zones.

The microstructure of the [100] penetrator is quite different from the shear band pattern seen in the other orientations. Etching of the polished surface delineated an extended pattern of fine cracks with a separation on the order of 0.1 mm extending throughout the sample (Figure 4). Superimposed on this is a more irregular pattern of cracks and fractures on a larger scale. Both of these crack and fracture patterns extend throughout the residual rod and into the back extrusion region as well (Figure 5). Only in limited areas are deformation bands observed, and the single crystal character is largely maintained through the initial flow until recrystallization occurs in the back extrusion region.

3. TRANSMISSION MICROSCOPY

Specimens were prepared for transmission microscopy by standard techniques. After cutting thin wafers from the bulk material by slow-speed diamond cutting, discs were spark machined and then hand ground to 50–100 μm. Final thinning was done with 2% NaOH solution at 40 V using a jet polisher. A major problem was the tendency of the samples to breakup due to cracks, inhomogeneities, etc., which occurred during the final stages of preparation. Both longitudinal and transverse sections were made, but the efforts to produce transverse samples met with more limited success.

Microscopy was done with a Phillips EM 300 at 100 kV and a Phillips EM 430 at 300 kV. Burgers vectors, line directions, and habit planes of the observed dislocation arrays were characterized by systematic contrast experiments under many different two-beam diffraction conditions. The Burgers vectors were determined from the g.b = 0 condition, as well as by the contrast shown by the dislocations when g.b = 1, 2, or more. Although the general location from which the discs were taken was documented, due to time constraints, it was not feasible to maintain unique reference coordinates during specimen preparation. Thus, the

Figure 4. Crack Pattern in [100] Residual Penetrator.

Figure 5. Microstructure of [100] Penetrator Network of Fine Cracks in the Back Extruded Region.

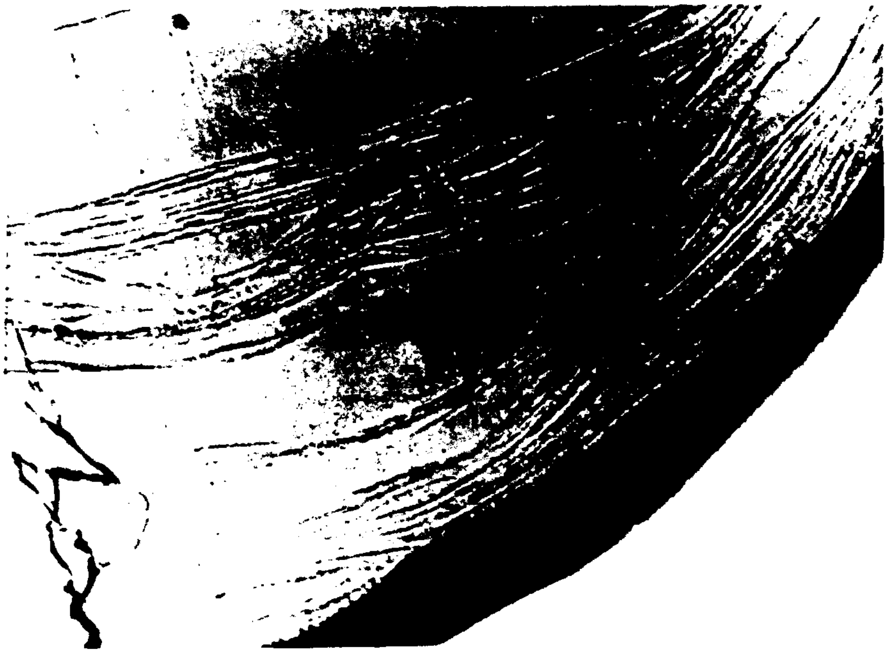

Figure 2. Optical Micrograph of Flow Pattern in [111] Penetrator Showing Unrecrystallized Material Surrounded by Shear Bands.

Figure 3. Optical Micrograph of [111] Penetrator Showing Shear Band Extending Into Residual Rod.

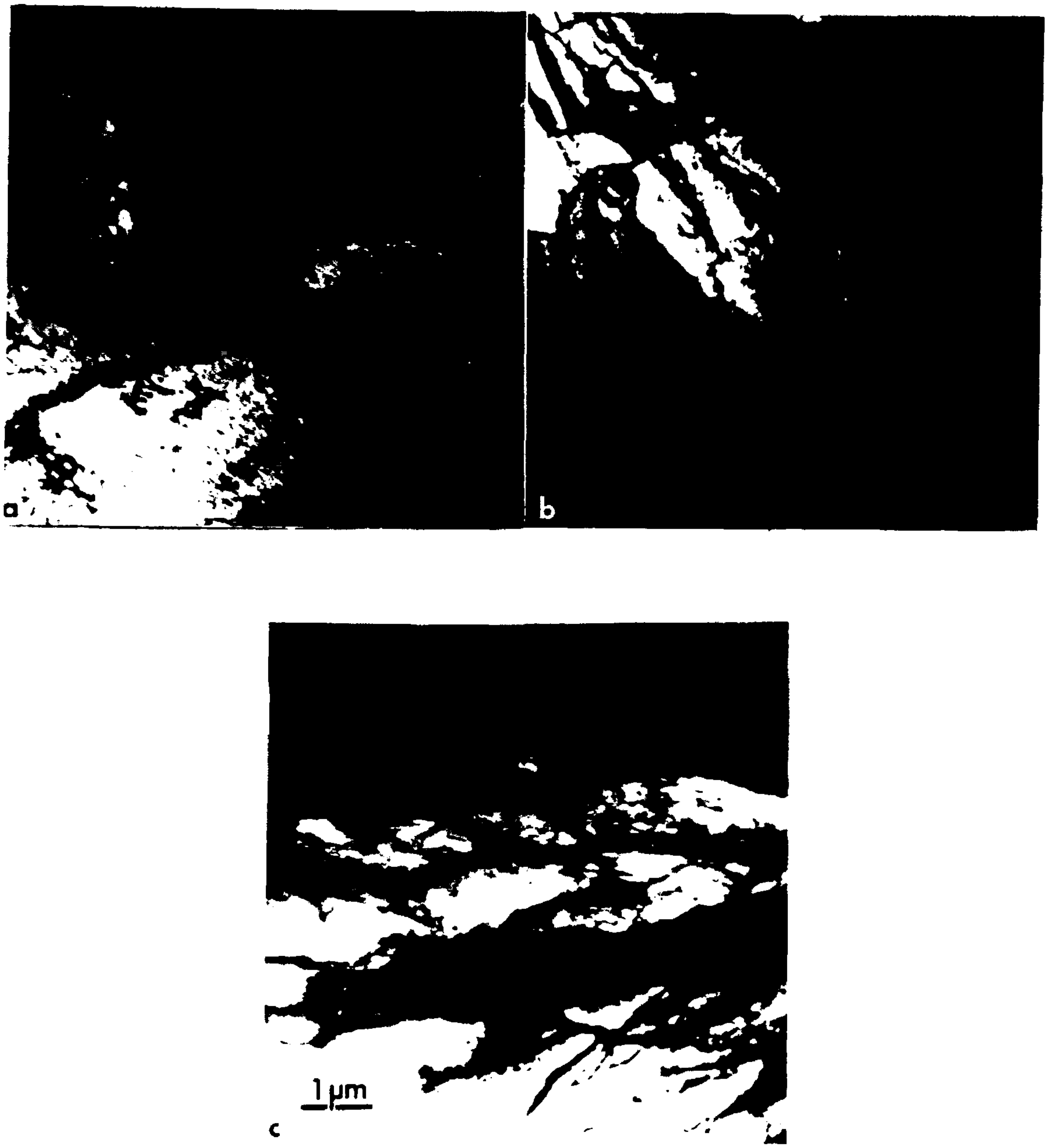

Figure 6. Dislocation Arrangement in [100] Penetrator Showing: (a) Initial Stage of Subgrain Formation, (b) Formation of Well-Defined Grains and (c) Formation of Elongated Grains.

crystallographic directions assigned during the analysis are arbitrary and cannot be correlated with the original penetrator or stress axes.

• TEM Results. A wide variety of microstructures was observed. This is to be expected from the inhomogeneity of the deformation process previously noted, and also from the general flow pattern in which severely worked material extrudes back adjacent to the remaining undeformed penetrator. However, certain microstructural patterns were generally observed. Dislocations were found with Burgers vectors of 1/2<111>. No other type of defect which could produce deformation was found. The dislocations polygonized the crystal by forming grain boundaries. Recrystallization of the grains removed the dense dislocation networks and was seen in material a few hundreds of micrometers from regions which appeared to have been freshly deformed. This process is illustrated in the sequence of micrographs in Figures 6a, 6b, and 6c from a region near the penetrator/target interface of the [100] penetrator. In Figure 6a, the dislocations form dense arrays which are the basis for subgrain formation. Well-defined grain boundaries have begun to form in Figure 6b and, in Figure 6c, elongated grains have formed with a high density of dislocations within themselves. Figure 7 shows a recrystallized region from the [111] penetrator with well-defined grains of different orientation and few interior dislocations. Similar general microstructure occurred in all penetrators, but the dislocation networks at subgrain boundaries were significantly different for each orientation, which was indicative of their different dislocation generation mechanisms. Examples for each orientation follow.

The dislocation network from a region of the [100] penetrator close to that of Figure 6 is shown in Figure 8. Four sets of dislocations labelled A–D dominate the microstructure. Detailed contrast analysis showed these dislocations to have four distinct Burgers vectors of the type 1/2<111> and to be either pure screws or mixed dislocations with a large screw component. The habit planes of the dislocations were either {110} or {112}.

The general appearance of a longitudinal specimen taken from the [111] penetrator near the outer circumference is shown in Figure 9. Subgrain boundaries containing a dense, orderly array of dislocations have formed. An adjacent region containing a dislocation network shown in Figures 10a, 10b, and 10c was analyzed in detail. The dislocation types A, B, and C have three distinct Burgers vectors of type 1/2 <111>. Figure 10a shows the complete

Figure 7. Recrystallized Region Showing Well-Defined Grains With Few or No Dislocations Within the Grains.

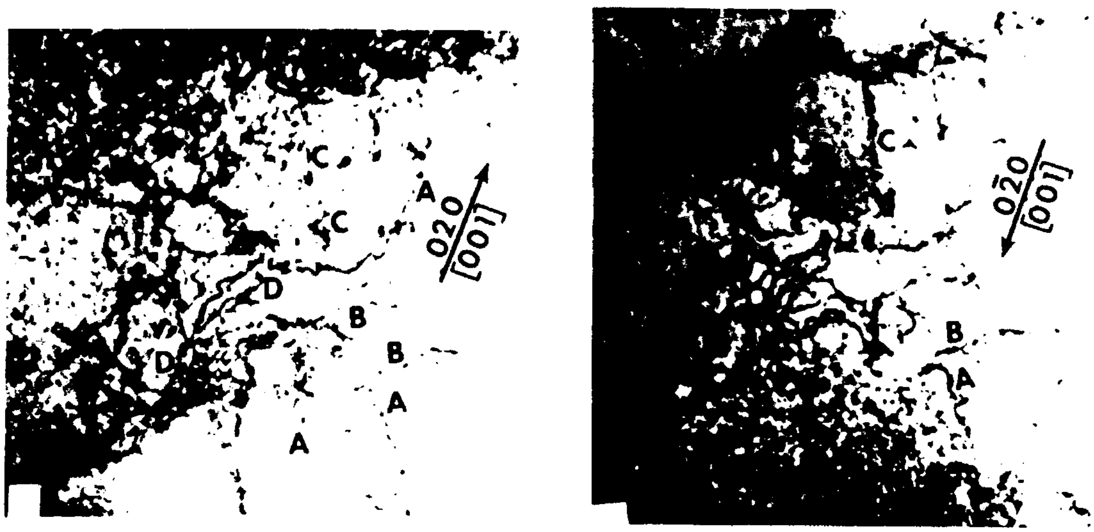

Figure 8. Dislocation Network in Regions Close to That Shown in Figure 6.

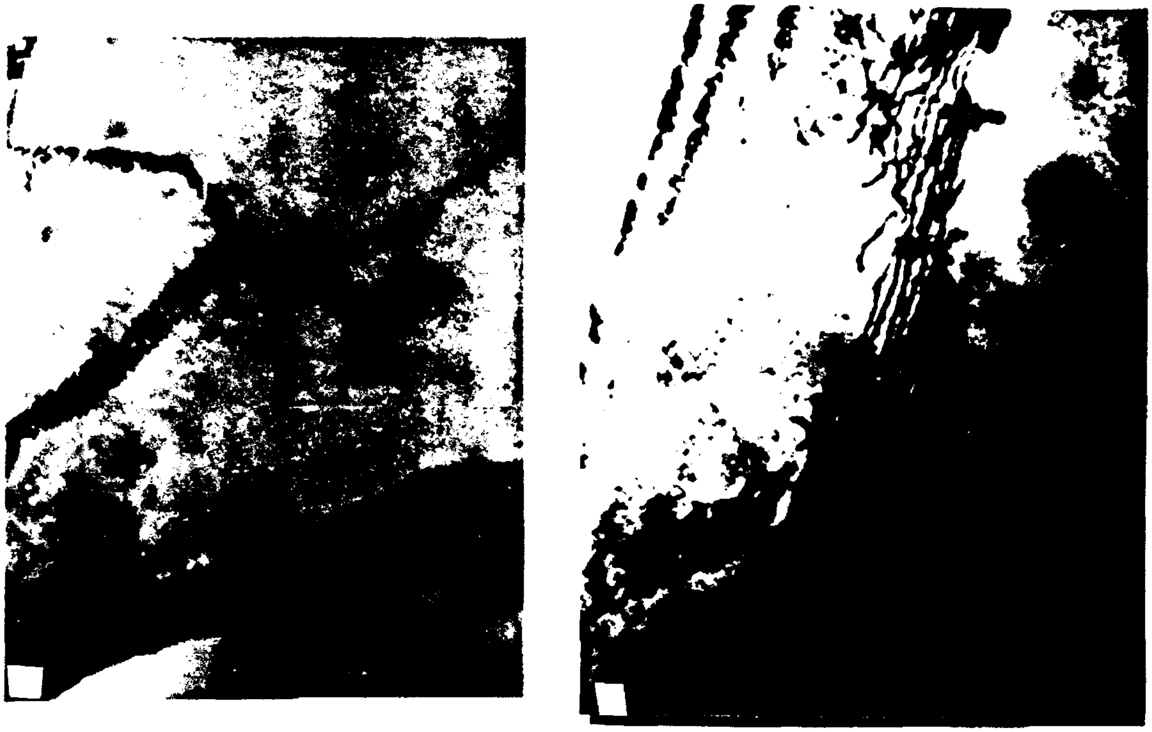

Figure 9. TEM Micrograph of [111] Penetrator Near the Outer Circumference.

Figure 10. TEM Micrograph of [111] Penetrator Showing the Dislocations as Either Pure Screws of Mixed Dislocations Containing Large Components.

network, while Figures 10b and 10c show A and B, respectively, out of contrast. Analysis of the line directions and habit planes shows that A and B are either pure screws or mixed dislocations containing large screw components.

The morphology of dislocation arrays in the [110] penetrator is shown in Figures 11a (elongated grains with a high density of dislocations) and 11b (small, also recrystallized grains of low dislocation density). An adjacent region was analyzed for dislocations, as shown in Figures 12a, 12b, and 12c. Three similar types of dislocations labelled A, B, and C dominate the microstructure. Analysis showed that each of these has a unique Burgers vector of type 1/2<111>, and that the long, straight dislocations of types A and B are pure screws having Burgers vectors (and line directions) $[11\bar{1}]$ and $[1\bar{1}1]$, respectively. Upon closer examination, both of these dislocation types are seen to contain short segments which are perpendicular to the principal line direction, as seen in Figure 12b for diffraction condition $0\bar{1}1$g [311]. The arrowed segments of the dislocations A disappear for diffracting condition $(\bar{1}01)$g[131] (Figure 12c) and, thus, have u~[131], which is also close to [211]. Thus, they are pure edge dislocations lying on (211) or $(1\bar{1}0)$ slip planes. Similarly, the arrowed segments of dislocations B disappear for $(\bar{2}1\bar{1})$g[001] (Figure 12d) and, thus, have u~[311], making them pure edge dislocations lying on $(21\bar{1})$ which is not far from the $(2\bar{1}1)$ and $(1\bar{1}0)$ slip planes of the dislocations A. The habit planes for the C dislocations were not determined since the line directions were difficult to follow.

To summarize, in all three orientations, dislocations of type 1/2 <111> were found, and no defects such as twins or stacking faults were observed. However, the dislocation networks varied as a function of orientation. For the [100] orientation, the arrays tended to be tangled and disorderly, as would be produced by the motion of screw dislocations or mixed dislocations with a large screw component. For the [110] orientation, an extensive and moderately orderly array containing many long, straight pure screw dislocations with edge segments at the ends occurred. This type of structure is typical of that left by pure edge dislocations passing through the crystal. The networks in the [111] crystal were quite orderly, but the dislocations tended to be wavy or bowed, like those seen in the [100]. Such dislocations tend to be produced by the motion of screws or mixed dislocations with strong screw character.

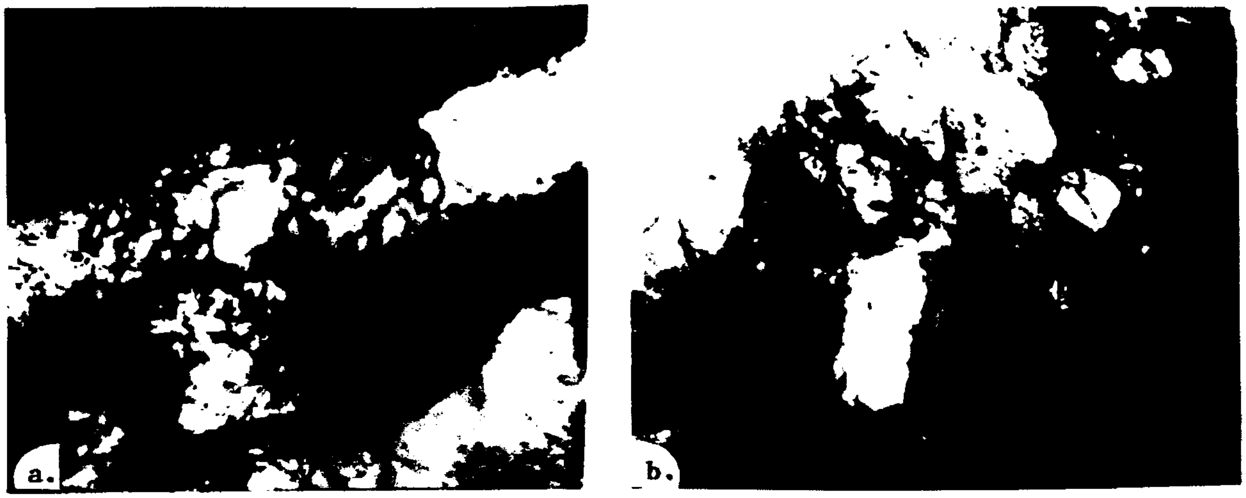

Figure 11. General Microstructure of Deformed [110] Penetrator Showing (a) Heavily Dislocated Grains and (b) Some Recrystallization Which Has Produced Small Grains of Low Dislocation Density.

4. CONCLUSIONS

The combined results described above provide additional insight into the material flow processes occurring during penetration. Although a significant amount of research has been performed on the deformation of tungsten single crystals, there is still no coherent description of the deformation mechanisms or work-hardening behavior. The present study clearly shows that deformation proceeds by the generation and interaction of dislocations of Burgers vector 1/2 <111> to form dislocation networks, subboundaries, and eventually recrystallization. No other defects such as twins or stacking faults were observed.

Crystallographic symmetry governs the operative dislocation systems in the initiation of deformation, and this establishes the eventual continuing course of deformation. The dislocation networks for the [100] penetrator were tangled arrays of bowed or wavy dislocations, while the dislocations in the [111] were similar, but the arrays were more orderly.

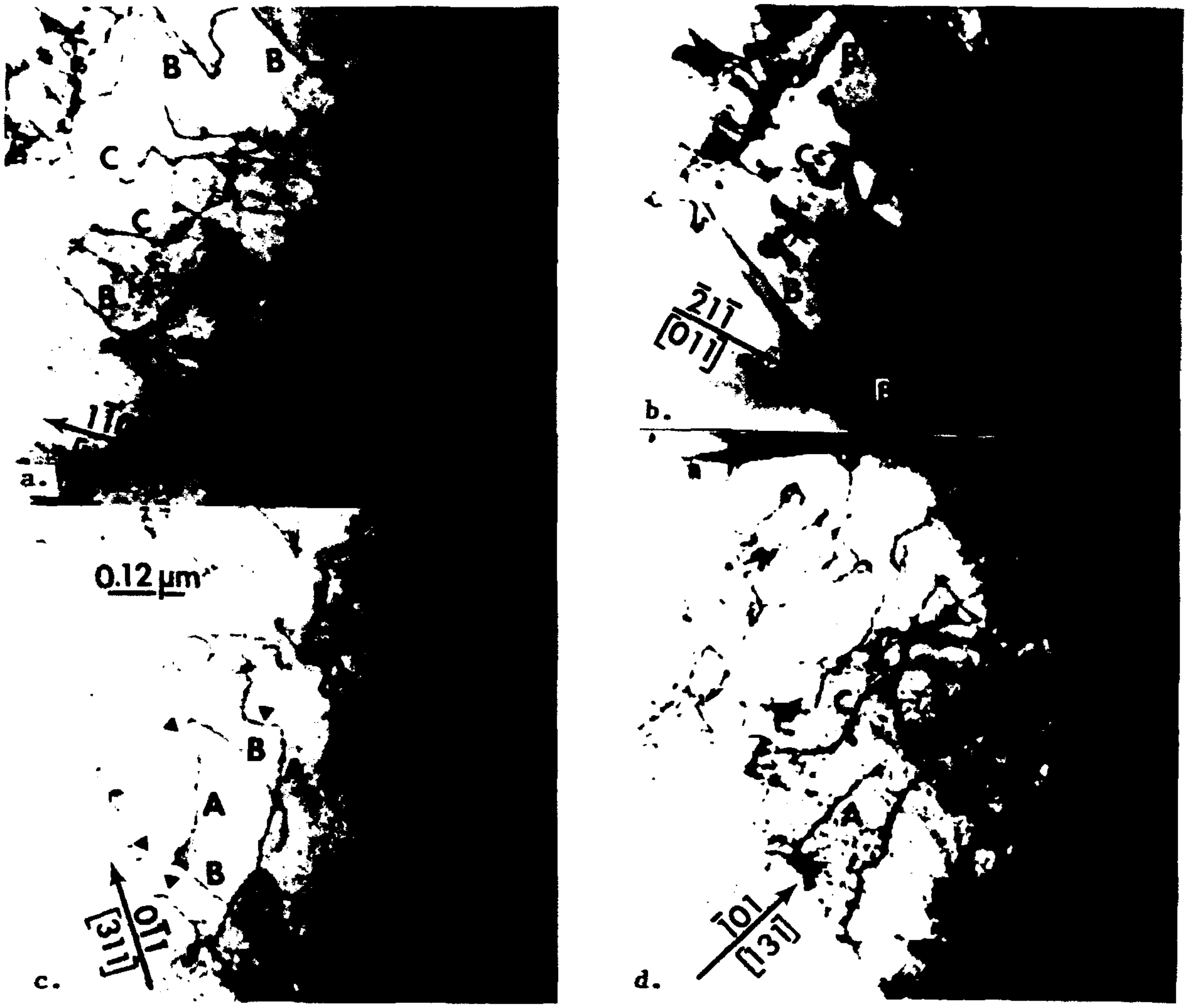

Figure 12. Dislocation Network in the [110] Penetrator Showing Two Beam Diffraction Conditions Which Put the Dislocation Groups Labelled A, B, C In or Out of Contrast.

In the [110] penetrator, straight screw dislocations with edge segments at the ends were found, implying that they were left behind by edge dislocations.

For the [100] (four-fold) axis, four <111> vectors lie at 54.7° from the stress axis. In addition, there are multiple {110} and also {112} planes which are favorably oriented for resolved shear stress, and the dislocations lying in these planes have a large screw component. This provides ample opportunity for dislocation motion and interaction, leading to the dense, wavy dislocation arrays observed here. This is in agreement with the work-hardening that was observed for this orientation previously (Beardmore and Hull 1965; Argon and Maloof 1966; Rose, Ferriss, and Wulf 1962).

In the [111] (3-fold) orientation, the three available <111> vectors are 70.5° from the stress axis. This results in resolved shear stresses on the slip systems that are relatively low. However, when the stresses become sufficient to initiate dislocation motion and interaction, orderly arrays are formed.

At the [110] (2-fold) axis, two <111> vectors lie in the plane normal to the stress axis, while the two operative <111> vectors are only 35° from the stress axis, and thus have a high resolved shear stress. It is apparent from the TEM analysis that slip by pure edge dislocations is operative. The overall behavior is highly asymmetric and in agreement with observations by other investigators (Argon and Maloof 1966; Rose, Ferris, and Wulf 1962).

Extensive cracking was observed macroscopically in the [100] penetrator. The reaction

$$a/2[111] + a/2[1\bar{1}\bar{1}] \Rightarrow a\,[100]$$

was suggested by Cottrell as a potential source for the initiation of cleavage cracks on {100}. Cleavage fractures on {100}, particularly in <100> oriented crystals, have been observed in bcc materials, including tungsten (Beardmore and Hull 1965).

As the material flows around the penetrator, it experiences intense working and increased temperature. As penetration occurs, the material experiences high stresses and temperature increases. When the material flows at high strains, a progressive process of recrystallization

and deformation undoubtedly occurs, leading to a highly textured substructure. This continuous process would also lead to the final microstructure where newly recrystallized, dislocation-free grains exist adjacent to regions which have freshly deformed.

Recrystallization of the grains removed the dense dislocation networks and was seen in close proximity to regions which appeared to have freshly deformed. The regions which are deforming at or near the penetrator/RHA interface are at relatively high temperature and there is sufficient energy to undergo recrystallization. It is likely that recrystallization of a given piece of material occurs a number of times during its course of flow from the head of the penetrator to the side wall of the cavity.

The general deformation mechanism and mass transfer from the penetrator to the walls of the cavity can be summarized as follows. The dislocations polygonized the single crystal by forming grain boundaries. The dislocations thread their way through the crystal and form dense arrays or subgrain boundaries and, eventually, they form elongated grains with a high density of dislocations within the grains. The flow of dislocations along these subgrain and grain boundaries produces a mass transfer in a direction within the plane of the boundary. Mass transfer along the subgrain boundaries reorients the grains to form well-defined grains and boundaries. Further mass transfer along the grain boundaries results in the grains becoming elongated in the direction of mass flow, similar to that of rolled or forged material.

The [100] and [111] oriented penetrators both produce deep penetration into RHA with the [100] orientation penetrating deepest. Both directions have symmetric multiple deformation systems which provide an even mass transfer to the wall of the cavity. The difference lies in the [100] producing dislocations on slip planes and the [111] producing pure screw dislocations which do not have a slip or glide plane. The [110] penetrator has only two-fold symmetry. This results in a less symmetric (elliptical) deformation cross section and also fewer available slip systems and lower work-hardening during flow. As a result, penetration depth is decreased.

In summary, it has been shown that crystal properties can have a significant effect on material behavior at the very high strain rates experienced during ballistic impact and penetration. While single crystals may not be generally employed as long rod penetrators,

this study suggests that crystal structure and texture could play a significant role in material performance and should be given consideration in the search for improved performance materials.

5. REFERENCES

Argon, A., and S. Maloof. "Plastic Deformation of Tungsten Single Crystals at Low Temperature." Acta Metallurgica, vol. 14, p. 1449, 1966.

Beardmore, P., and D. Hull. "Deformation and Fracture of Tungsten Single Crystals." Journal of Less-Common Metals, vol. 9, p. 168, 1965.

Bruchey, W. J., E. J. Horwath, and P. W. Kingman. "Orientation Dependence of Deformation and Penetration Behavior of Tungsten Single Crystal Rods." Tungsten and Tungsten Alloys: Recent Advances, A. Crowson, E. S. Chen, Eds. The Minerals, Metals, and Materials Society, Warrendale, PA, pp. 121–128, 1991.

Rose, R., D. Ferriss, and J. Wulf. "Yielding and Plastic Flow in Single Crystals of Tungsten." Trans. Metallurgical Society AIME, vol. 224, p. 981, 1962.

INTENTIONALLY LEFT BLANK.

No. of Copies	Organization
2	Administrator Defense Technical Info Center ATTN: DTIC-DDA Cameron Station Alexandria, VA 22304-6145
1	Commander U.S. Army Materiel Command ATTN: AMCAM 5001 Eisenhower Ave. Alexandria, VA 22333-0001
1	Director U.S. Army Research Laboratory ATTN: AMSRL-OP-CI-AD, Tech Publishing 2800 Powder Mill Rd. Adelphi, MD 20783-1145
1	Director U.S. Army Research Laboratory ATTN: AMSRL-OP-CI-AD, Records Management 2800 Powder Mill Rd. Adelphi, MD 20783-1145
2	Commander U.S. Army Armament Research, Development, and Engineering Center ATTN: SMCAR-IMI-I Picatinny Arsenal, NJ 07806-5000
2	Commander U.S. Army Armament Research, Development, and Engineering Center ATTN: SMCAR-TDC Picatinny Arsenal, NJ 07806-5000
1	Director Benet Weapons Laboratory U.S. Army Armament Research, Development, and Engineering Center ATTN: SMCAR-CCB-TL Watervliet, NY 12189-4050
(Unclass. only)1	Commander U.S. Army Rock Island Arsenal ATTN: SMCRI-IMC-RT/Technical Library Rock Island, IL 61299-5000
1	Director U.S. Army Aviation Research and Technology Activity ATTN: SAVRT-R (Library) M/S 219-3 Ames Research Center Moffett Field, CA 94035-1000

No. of Copies	Organization
1	Commander U.S. Army Missile Command ATTN: AMSMI-RD-CS-R (DOC) Redstone Arsenal, AL 35898-5010
1	Commander U.S. Army Tank-Automotive Command ATTN: ASQNC-TAC-DIT (Technical Information Center) Warren, MI 48397-5000
1	Director U.S. Army TRADOC Analysis Command ATTN: ATRC-WSR White Sands Missile Range, NM 88002-5502
1	Commandant U.S. Army Field Artillery School ATTN: ATSF-CSI Ft. Sill, OK 73503-5000
(Class. only)1	Commandant U.S. Army Infantry School ATTN: ATSH-CD (Security Mgr.) Fort Benning, GA 31905-5660
(Unclass. only)1	Commandant U.S. Army Infantry School ATTN: ATSH-CD-CSO-OR Fort Benning, GA 31905-5660
1	WL/MNOI Eglin AFB, FL 32542-5000
	Aberdeen Proving Ground
2	Dir, USAMSAA ATTN: AMXSY-D AMXSY-MP, H. Cohen
1	Cdr, USATECOM ATTN: AMSTE-TC
1	Dir, ERDEC ATTN: SCBRD-RT
1	Cdr, CBDA ATTN: AMSCB-CI
1	Dir, USARL ATTN: AMSRL-SL-I
10	Dir, USARL ATTN: AMSRL-OP-CI-B (Tech Lib)

No. of Copies	Organization
1	Director U.S. Army Research Office ATTN: A. Crowson P.O. Box 12211 Research Triangle Park, NC 27709-2211
1	Director U.S. Army Research Office ATTN: I. Iyer P.O. Box 12211 Research Triangle Park, NC 27709-2211
1	Director U.S. Army Research Office ATTN: J. Wu P.O. Box 12211 Research Triangle Park, NC 27709-2211
3	Director U.S. Army Research Laboratory Materials Directorate ATTN: AMSRL-MA, S. Chou J. Dandekar Watertown, MA 02172-0001
1	Commander U.S. Army Tank-Automotive Research and Development Center ATTN: AMSTA-RSS Warren, MI 48397-5000
1	U.S. Naval Academy Department of Mathematics ATTN: R. Malek-Madani Annapolis, MD 21402
1	Air Force Armament Laboratory ATTN: J. Foster Eglin AFB, FL 32542-5438
1	Air Force Wright Aeronautical Laboratories Air Force Systems Command Materials Laboratory ATTN: T. Nicholas Wright-Patterson AFB, OH 45433

No. of Copies	Organization
3	Director Sandia National Laboratories ATTN: L. Davison W. Herrmann P. Chen P.O. Box 5800 Albuquerque, NM 87285-5800
1	Director Sandia National Laboratories ATTN: S. Passman P.O. Box 5800 Albuquerque, NM 87285-5800
1	Director Sandia National Laboratories ATTN: M. Forrestal P.O. Box 5800 Albuquerque, NM 87285-5800
1	Director Sandia National Laboratories ATTN: D. Bammann Livermore, CA 94550
1	National Institute of Science and Technology ATTN: T. Burns Technology Building, Room A151 Gaithersburg, MD 20899
1	University of Missouri-Rolla Dept. of Mechanical and Aerospace Engineering ATTN: R. Batra Rolla, MO 65401-0249
1	California Institute of Technology Division of Engineering and Applied Science ATTN: J. Knowles Pasadena, CA 91102
1	Massachusetts Institute of Technology Dept. of Mechanical Engineering ATTN: L. Anand Cambridge, MA 02139

No. of Copies	Organization
2	Rennselaer Polytechnic Institute Department of Mechanical Engineering ATTN: E. Lee E. Krempl Troy, NY 12181
1	Rennselaer Polytechnic Institute Dept. of Computer Science ATTN: J. Flaherty Troy, NY 12181
1	Brown University Division of Engineering ATTN: R. Clifton Providence, RI 02912
1	Brown University Division of Engineering ATTN: B. Freund Providence, RI 02912
1	Brown University Division of Engineering ATTN:A Needleman Providence, RI 02912
1	Brown University Division of Applied Mathematics ATTN: C. Dafermos Providence, RI 02912
1	Carnegie-Mellon University Dept. of Mathematics ATTN: D. Owen Pittsburg, PA 15213
1	Carnegie-Mellon University Dept. of Mathematics ATTN: M. Gurtin Pittsburg, PA 15213
1	Cornell University Dept. of Theoretical and Applied Mechanics ATTN: J. Jenkins Ithaca, NY 14850
1	Cornell University Dept. of Theoretical and Applied Mechanics ATTN: P. Rosakis Ithaca, NY 14850

No. of Copies	Organization
1	Cornell University Dept. of Theoretical and Applied Mechanics ATTN: W. Sachse Ithaca, NY 14850
1	Cornell University Dept. of Theoretical and Applied Mechanics ATTN: T. Healey Ithaca, NY 14850
1	Cornell University Dept. of Theoretical and Applied Mechanics ATTN: A. Zehnder Ithaca, NY 14850
1	Harvard University Division of Engineering and Applied Physics ATTN: J. Rice Cambridge, MA 02138
1	Harvard University Division of Engineering and Applied Physics ATTN: J. Hutchinson Cambridge, MA 02138
1	North Carolina State University Dept. of Civil Engineering ATTN: Y. Horie Raleigh, NC 27607
1	Rice University Dept of Mathematical Sciences ATTN: C. C. Wang P.O. Box 1892 Houston, TX 77001
1	The Johns Hopkins University Dept. of Mechanical Engineering Latrobe Hall ATTN: W. Sharp 34th and Charles Streets Baltimore, MD 21218
1	The Johns Hopkins University Dept. of Mechanical Engineering Latrobe Hall ATTN: G. Bao 34th and Charles Streets Baltimore, MD 21218

No. of Copies	Organization
1	The Johns Hopkins University Dept. of Mechanical Engineering Latrobe Hall ATTN: K. T. Ramesh 34th and Charles Streets Baltimore, MD 21218
1	The Johns Hopkins University Dept. of Mechanical Engineering Latrobe Hall ATTN: A. Douglas 34th and Charles Streets Baltimore, MD 21218
1	University of California at Santa Barbara Dept of Materials Science ATTN: A. Evans Santa Barbara, CA 93106
1	University of California at San Diego Dept. of Applied Mechanics and Engineering Sciences ATTN: S. Nemat-Nasser La Jolla, CA 92093
1	University of California at San Diego Dept. of Applied Mechanics and Engineering Sciences ATTN: M. Meyers La Jolla, CA 92093
1	University of California at San Diego Dept. of Applied Mechanics and Engineering Sciences ATTN: X. Markenscoff La Jolla, CA 92093
1	University of California at San Diego Dept. of Applied Mechanics and Engineering Sciences ATTN: A. Hoger La Jolla, CA 92093

No. of Copies	Organization
1	University of California at San Diego Dept. of Applied Mechanics and Engineering Sciences ATTN: R. Asaro La Jolla, CA 92093
1	Northwestern University Dept. of Applied Mathematics ATTN: W. Olmstead Evanston, IL 60201
1	University of Florida Dept. of Engineering Science and Mechanics ATTN: L. Malvern Gainesville, FL 32601
1	University of Florida Dept. of Engineering Science and Mechanics ATTN: D. Drucker Gainesville, FL 32601
1	University of Florida Dept. of Engineering Science and Mechanics ATTN: M. Eisenberg Gainesville, FL 32601
1	University of Houston Dept. of Mechanical Engineering ATTN: L. Wheeler Houston, TX 77004
1	University of Illinois Dept. of Theoretical and Applied Mechanics ATTN: D. Carlson Urbana, IL 61801
1	University of Illinois at Chicago Circle Dept. of Engineering, Mechanics, and Metallurgy ATTN: T. Ting P.O. Box 4348 Chicago, IL 60680

No. of Copies	Organization
1	University of Kentucky Dept. of Engineering Mechanics ATTN: O. Dillon, Jr. Lexington, KY 40506
1	University of Maryland Dept. of Mathematics ATTN: S. Antman College Park, MD 20742
1	University of Maryland Dept. of Mathematics ATTN: T. Liu College Park, MD 20742
1	University of Minnesota Dept. of Aerospace Engineering and Mechanics ATTN: R. Fosdick 110 Union Street SE Minneapolis, MN 55455
1	University of Minnesota Dept. of Aerospace Engineering and Mechanics ATTN: R. James 110 Union Street SE Minneapolis, MN 55455
1	University of Oklahoma School of Aerospace, Mechanical and Nuclear Engineering ATTN: C. Bert Norman, OK 73019
1	University of Texas Dept. of Engineering Mechanics ATTN: J. Oden Austin, TX 78712
1	University of Washington Dept. of Aeronautics and Astronautics ATTN: I. Fife 206 Guggenheim Hall Seattle, WA 98195

No. of Copies	Organization
1	University of Maryland Dept. of Mechanical Engineering ATTN: R. Armstrong College Park, MD 20742
1	University of Maryland Dept. of Mechanical Engineering ATTN: J. Dally College Park, MD 20742
1	University of Wyoming Dept. of Mathematics ATTN: R. Ewing P.O. Box 3036 University Station Laramie, WY 82070
1	Washington State University Mechanical and Materials Engineering ATTN: H. M. Zbib Pullman, WA 99164
1	Yale University Dept. of Mechanical Engineering ATTN: E. Onat 400 Temple Street New Haven, CT 96520
1	Southwest Research Institute Department of Mechanical Sciences ATTN: U. Lindholm 8500 Culebra Road San Antonio, TX 02912
1	Southwest Research Institute Department of Mechanical Sciences ATTN: C. Anderson 8500 Culebra Road San Antonio, TX 02912
1	Southwest Research Institute Department of Mechanical Sciences ATTN: J. Lankford 8500 Culebra Road San Antonio, TX 02912

No. of Copies	Organization
1	The Johns Hopkins University Materials Science and Engineering ATTN: R. E. Green 102 Maryland Hall Baltimore, MD 21218
1	University of Nebraska Engineering Mechanics ATTN: M. Beatty 212 Bancroft Hall Lincoln, NE 68588
1	Oklahoma State University ATTN: R. M. Bowen 101 Whitehurst Hall Stillwater, OK 74078
1	University of Maryland Baltimore County Mechanical Engineering ATTN: A. Khan Baltimore, MD 21228
1	University of Wisconsin Dept. of Mathematics ATTN: A. Tzavaras Madison, WI 53706
1	California Institute of Technology ATTN: G. Ravichandran Mail Code 105-50 Pasadena, CA 91125
1	State University of New York at Stony Brook Applied Mathematics and Statistics P138A Mathematics ATTN: J. Glimm Stony Brook, NY 11794
1	University of Virginia Dept. of Applied Mathematics ATTN: C. O. Horgan Thornton Hall Charlottesville, VA 22903

No. of Copies	Organization
1	Drexel University Dept. of Materials Engineering ATTN: H. C. Rogers Philadelphia, PA 18104
1	SRI International ATTN: D. Curran 333 Ravenswood Avenue Menlo Park, CA 94025
1	SRI International ATTN: R. Shockey 333 Ravenswood Avenue Menlo Park, CA 94025
1	SRI International ATTN: L. Seaman 333 Ravenswood Avenue Menlo Park, CA 94025

USER EVALUATION SHEET/CHANGE OF ADDRESS

This Laboratory undertakes a continuing effort to improve the quality of the reports it publishes. Your comments/answers to the items/questions below will aid us in our efforts.

1. ARL Report Number ARL-TR-133 Date of Report May 1993

2. Date Report Received ______________________________

3. Does this report satisfy a need? (Comment on purpose, related project, or other area of interest for which the report will be used.) ______________________________

4. Specifically, how is the report being used? (Information source, design data, procedure, source of ideas, etc.) ______________________________

5. Has the information in this report led to any quantitative savings as far as man-hours or dollars saved, operating costs avoided, or efficiencies achieved, etc? If so, please elaborate. ______________________________

6. General Comments. What do you think should be changed to improve future reports? (Indicate changes to organization, technical content, format, etc.) ______________________________

CURRENT ADDRESS

Organization

Name

Street or P.O. Box No.

City, State, Zip Code

7. If indicating a Change of Address or Address Correction, please provide the Current or Correct address above and the Old or Incorrect address below.

OLD ADDRESS

Organization

Name

Street or P.O. Box No.

City, State, Zip Code

(Remove this sheet, fold as indicated, tape closed, and mail.)

(DO NOT STAPLE)

DEPARTMENT OF THE ARMY

OFFICIAL BUSINESS

BUSINESS REPLY MAIL
FIRST CLASS PERMIT No 0001, APG, MD

Postage will be paid by addressee

NO POSTAGE
NECESSARY
IF MAILED
IN THE
UNITED STATES

Director
U.S. Army Research Laboratory
ATTN: AMSRL-OP-CI-B (Tech Lib)
Aberdeen Proving Ground, MD 21005-5066